Supporting Information for "Drivers of Future Extratropical SST Variability Changes in the North Pacific"

Jacob L. Gunnarson[1], Malte F. Stuecker[1,2], and Sen Zhao[3]

[1]Department of Oceanography, University of Hawaiʻi at Mānoa, Honolulu, HI, USA
[2]International Pacific Research Center, University of Hawaiʻi at Mānoa, Honolulu, HI, USA
[3]Department of Atmospheric Sciences, University of Hawaiʻi at Mānoa, Honolulu, HI, USA

December 13, 2023

Contents of this file

- Supplementary Figures S1-S7

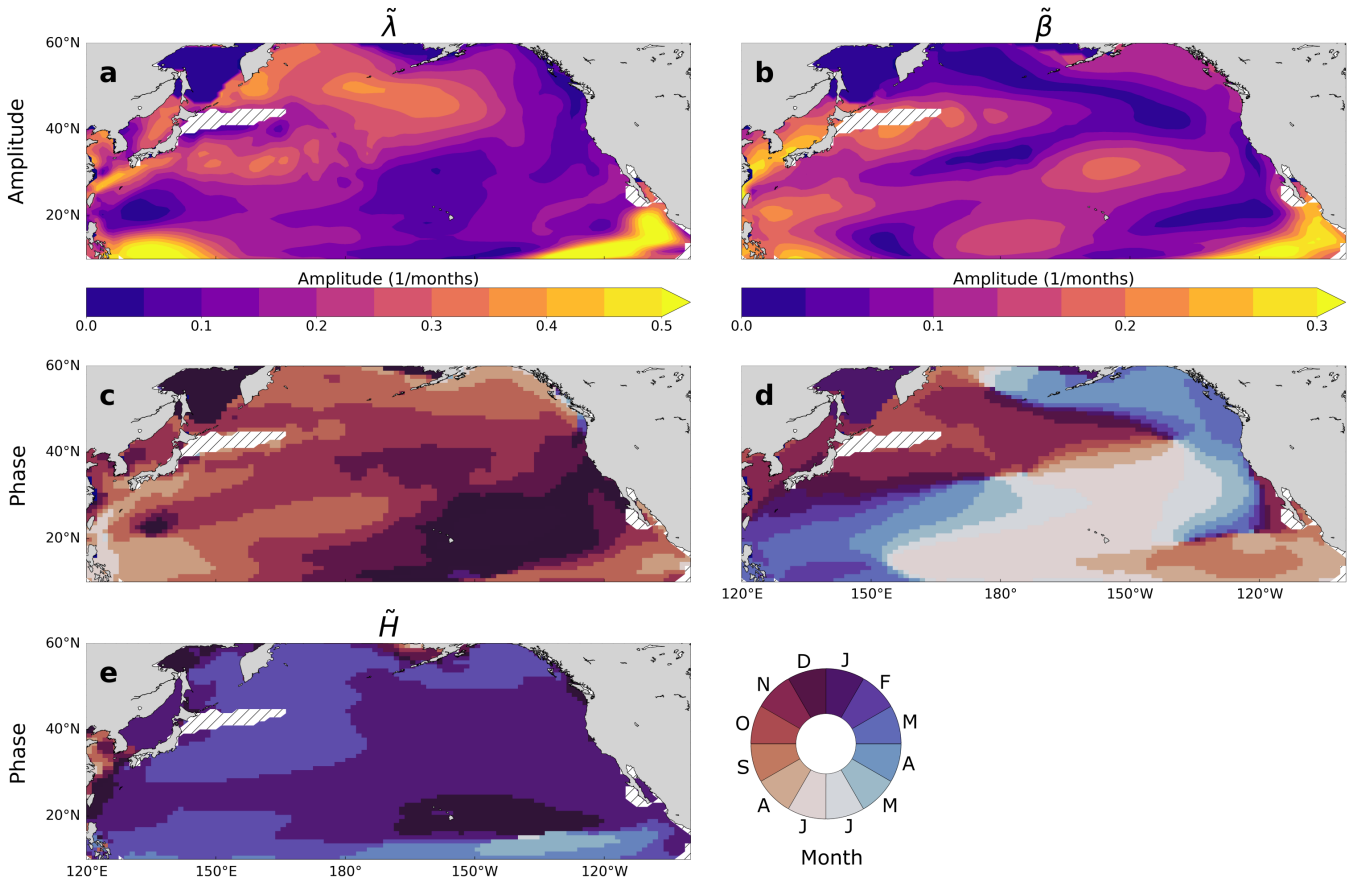

Supplementary Figure S1: Seasonal modulation of the the feedback coefficient $\tilde{\lambda}$ and ENSO teleconnection coefficient $\tilde{\beta}$ in CESM2-LE for 1960-2000. (a)-(b) Amplitude of $\tilde{\lambda}$ and $\tilde{\beta}$, defined as the absolute difference between the minimum and maximum values of each coefficient at each grid point. (c) The month in which $\tilde{\lambda}$ is most negative (i.e., the damping is strongest). (d) The month in which $\tilde{\beta}$ is largest. (e) The month in which the mixed layer depth climatology $\tilde{H}$ is deepest. Note the phase difference between $\tilde{\lambda}$ and $\tilde{H}$ over much of the North Pacific, suggesting that the seasonality of the air-sea heat flux feedbacks also contributes to the seasonality of $\tilde{\lambda}$. All parameters shown are ensemble means.

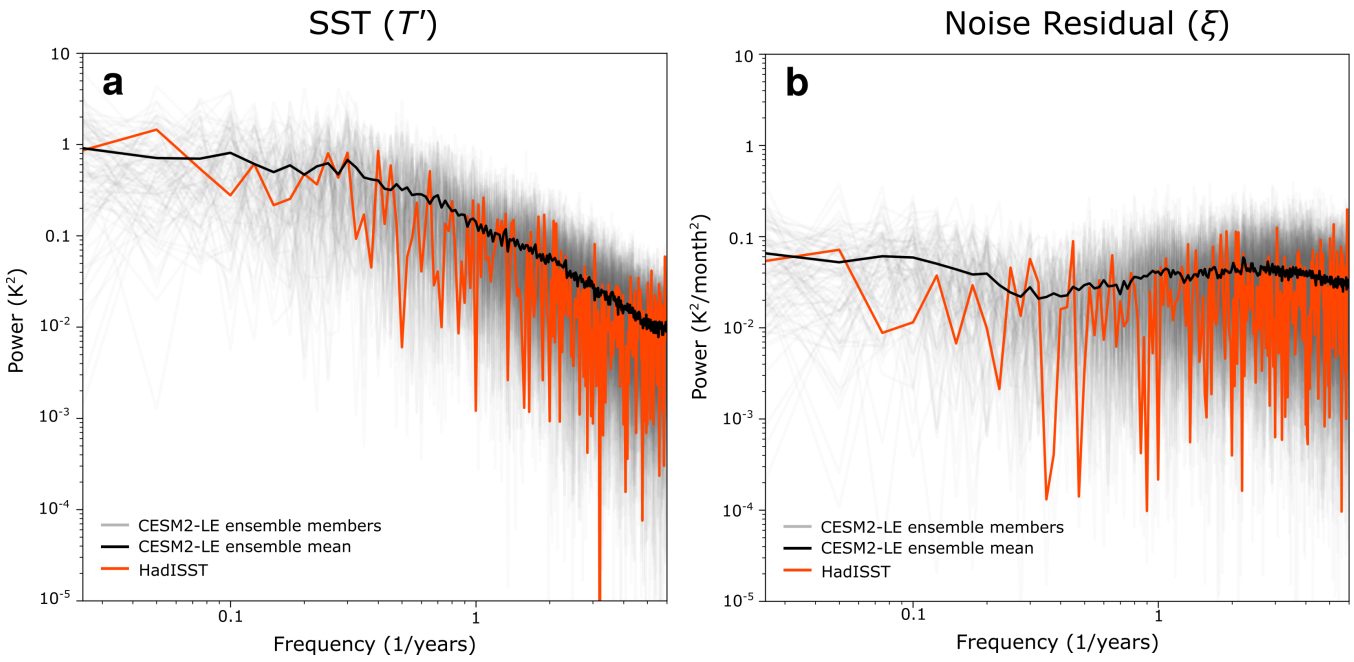

Supplementary Figure S2: Power spectra (computed via discrete FFT) of (a) SST anomalies and (b) the fit residual ξ for a representative locations in the North Pacific (40°N, 180°E) from 1960-2000. Individual ensemble members are shown as light grey lines, with a black line denoting the ensemble mean. The red line is the corresponding spectrum computed from HadISST at the same location and time period. The SST power spectrum exhibits Lorentzian spectra characteristic of local linear stochastic models such as Eq. 1 in the main text. The spectrum of the noise residual is nearly white (i.e., the power is independent of frequency), consistent with stochastic forcing from the atmosphere as proposed by Hasselmann (1976).

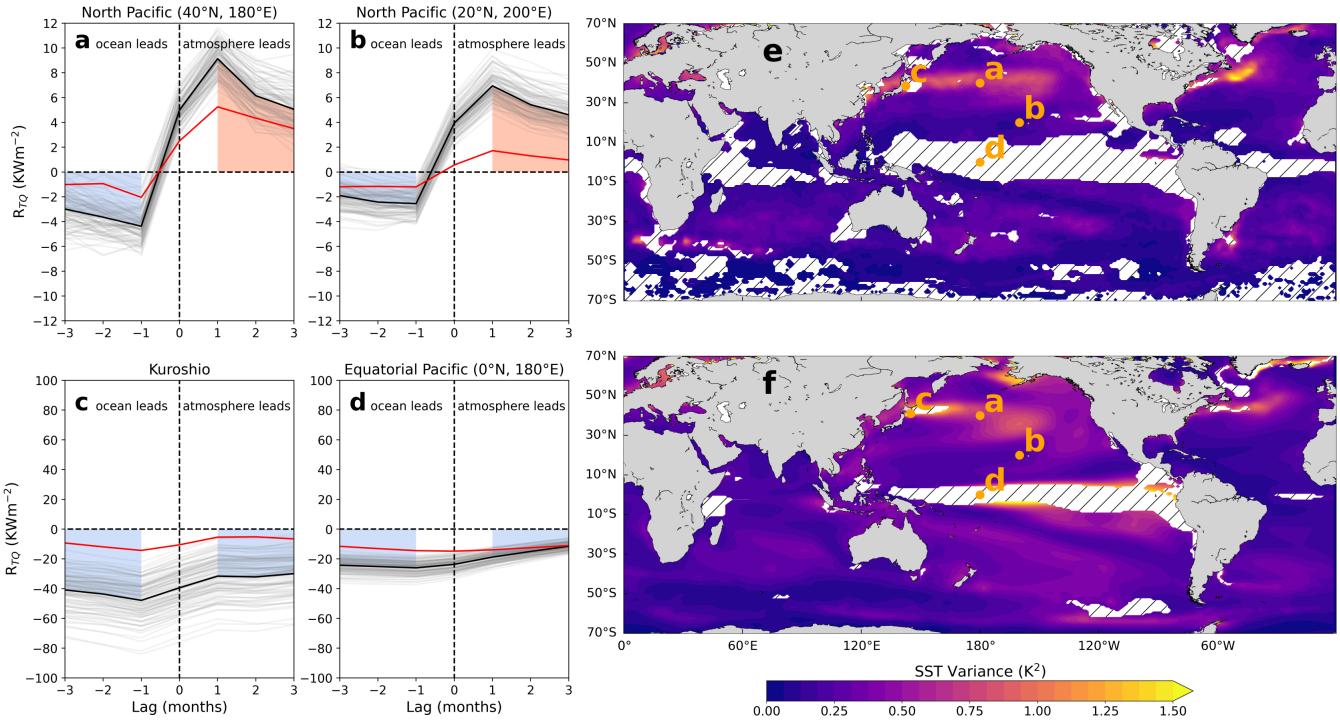

Supplementary Figure S3: The covariance of SST and air-sea heat flux anomalies R_{TQ} at four locations in CESM2-LE for 1960-2000: (a) and (b) representative locations in the North Pacific, (c) the Kuroshio current (41°N, 145°E for CESM2-LE and 142.5°N, 38.5°E), (d) the equatorial Pacific. Individual CESM2-LE ensemble members are shown as light grey lines, with a black line denoting the ensemble mean. The observed covariance (from HadISST, OAFLUX, and CERES EBAF) are shown as a red line. The area under the ensemble mean for lags of -1 to -3 months and 1 to 3 months is shaded blue if it is negative and red if it is positive. As discussed in the main text (Section 2.3) a location with an ensemble-mean $R_{TQ} < 0$ at negative lags (averaged over lags -3 to -1 months) and $R_{TQ} > 0$ at positive lags (averaged over lags 1 to 3 months) is well-described by a local linear stochastic model. The locations of (a) and (b) meet this criterion, while (c) and (d) do not.

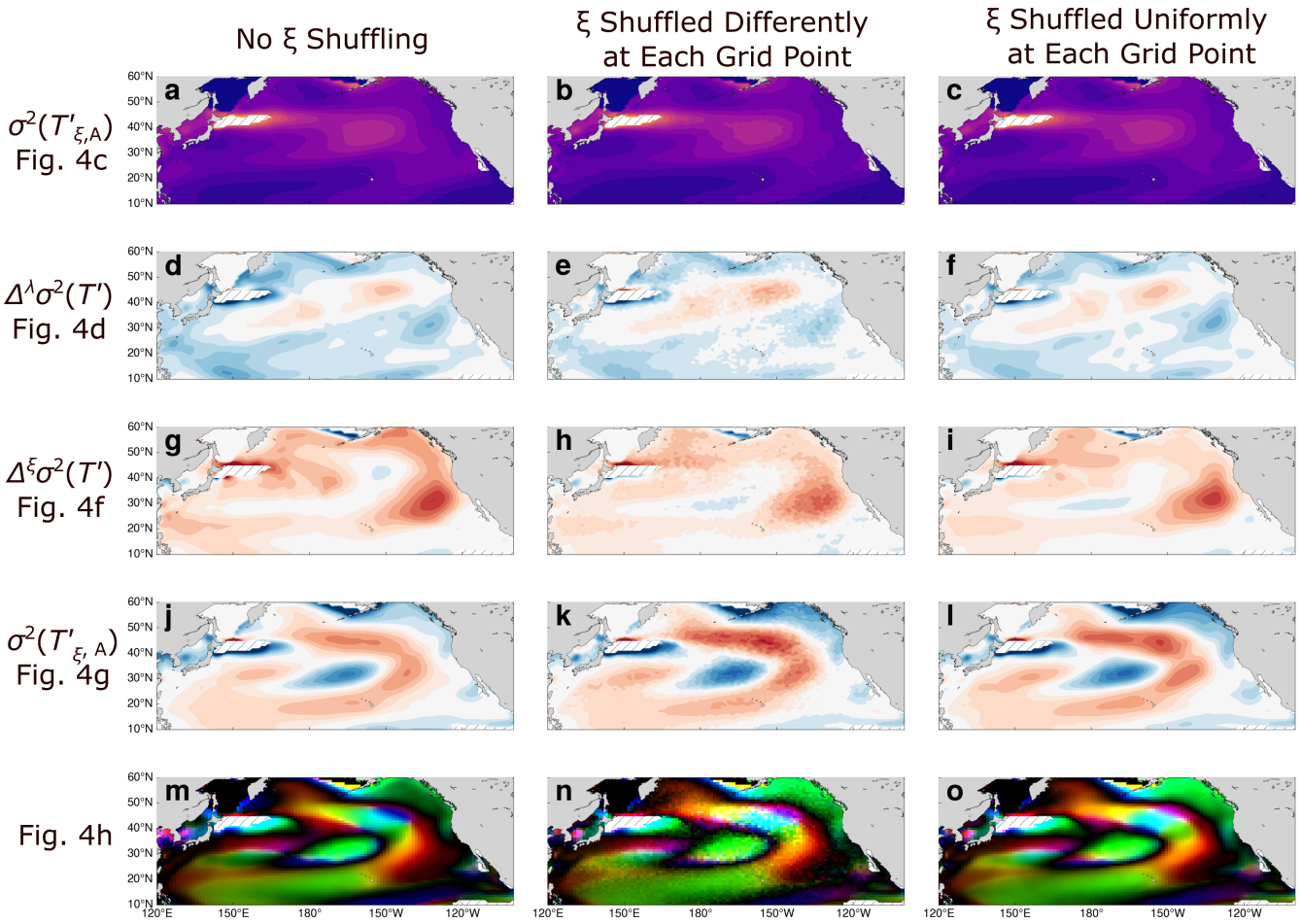

Supplementary Figure S4: The impact of different methods of shuffling the stochastic forcing ξ. The labels on the left refer to the corresponding panels in Figure 4 of the main text. *First column*: ξ was not shuffled, thus retaining both spatial and (slight) temporal correlations. *Second column*: ξ was randomly shuffled in time differently at each grid point and ensemble member, eliminating any temporal or spatial correlations. *Third column*: ξ was randomly shuffled in time uniformly at each grid point and ensemble, eliminating any temporal correlation while retaining spatial correlations (identical to the corresponding panels in Figure 4 in the main text). With both methods of shuffling, for each calendar month the year was randomly shuffled to retain the seasonality of the variance of the forcing.

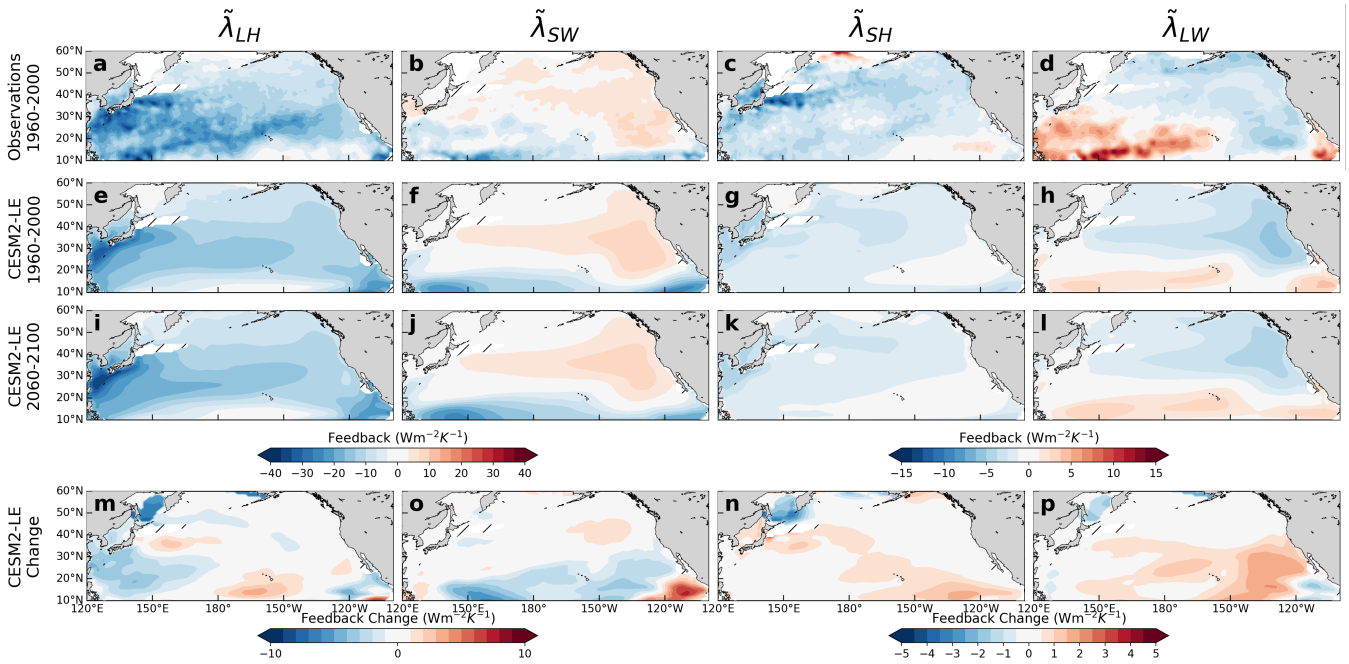

Supplementary Figure S5: SST feedbacks from the following heat flux components: latent heat feedback $\tilde{\lambda}^*_{\mathrm{LH}}$, sensible heat feedback $\tilde{\lambda}^*_{\mathrm{SH}}$, shortwave feedback $\tilde{\lambda}^*_{\mathrm{SW}}$, and longwave heat feedback $\tilde{\lambda}^*_{\mathrm{LW}}$. (a)-(d) Observations (HadISST, OAFLUX, CERES EBAF) for 1985-2022. (e)-(h) CESM2-LE for 1960-2000. (i)-(l) CESM2-LE for 1960-2000. (m)-(p) Change in CESM2-LE between 1960-2000 and 2060-2100.

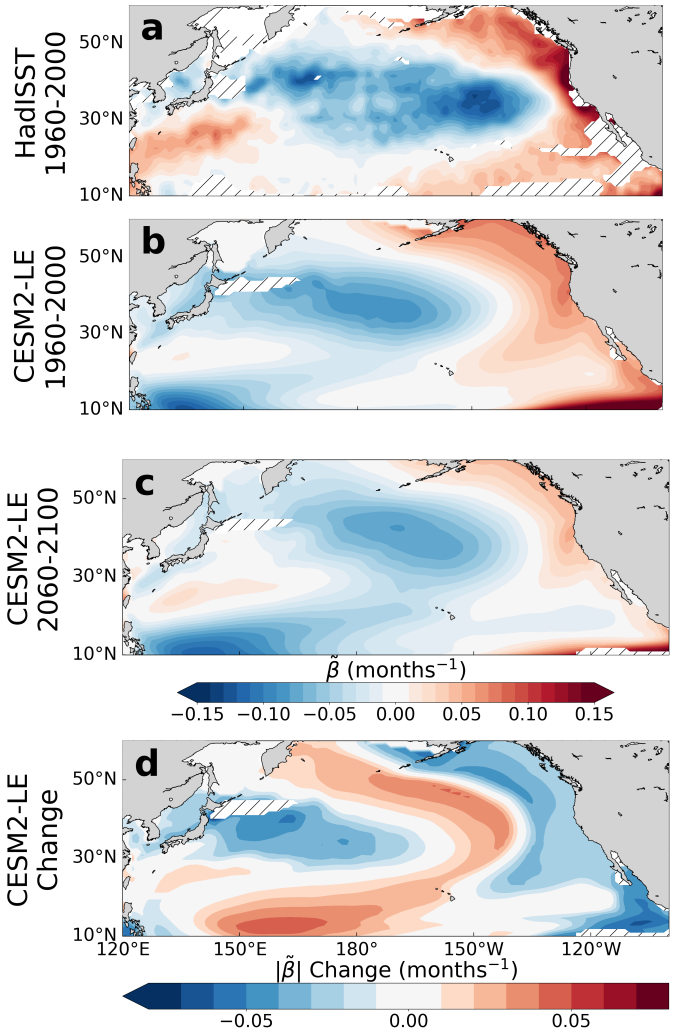

Supplementary Figure S6: The ENSO teleconnection coefficient $\tilde{\beta}$ from (a) HadISST for 1960-2000, (b) CESM2-LE for 1960-2000 and (c) 2060-2100, and (d) the change in the absolute magnitude of $\tilde{\beta}$ in CESM2-LE between the two time period. This figure is similar to the second column of Figure 2 in the main text, which showed the ENSO teleconnection coefficient multiplied by the Niño3.4 standard deviation $\tilde{\beta}\sigma$(Niño3.4).

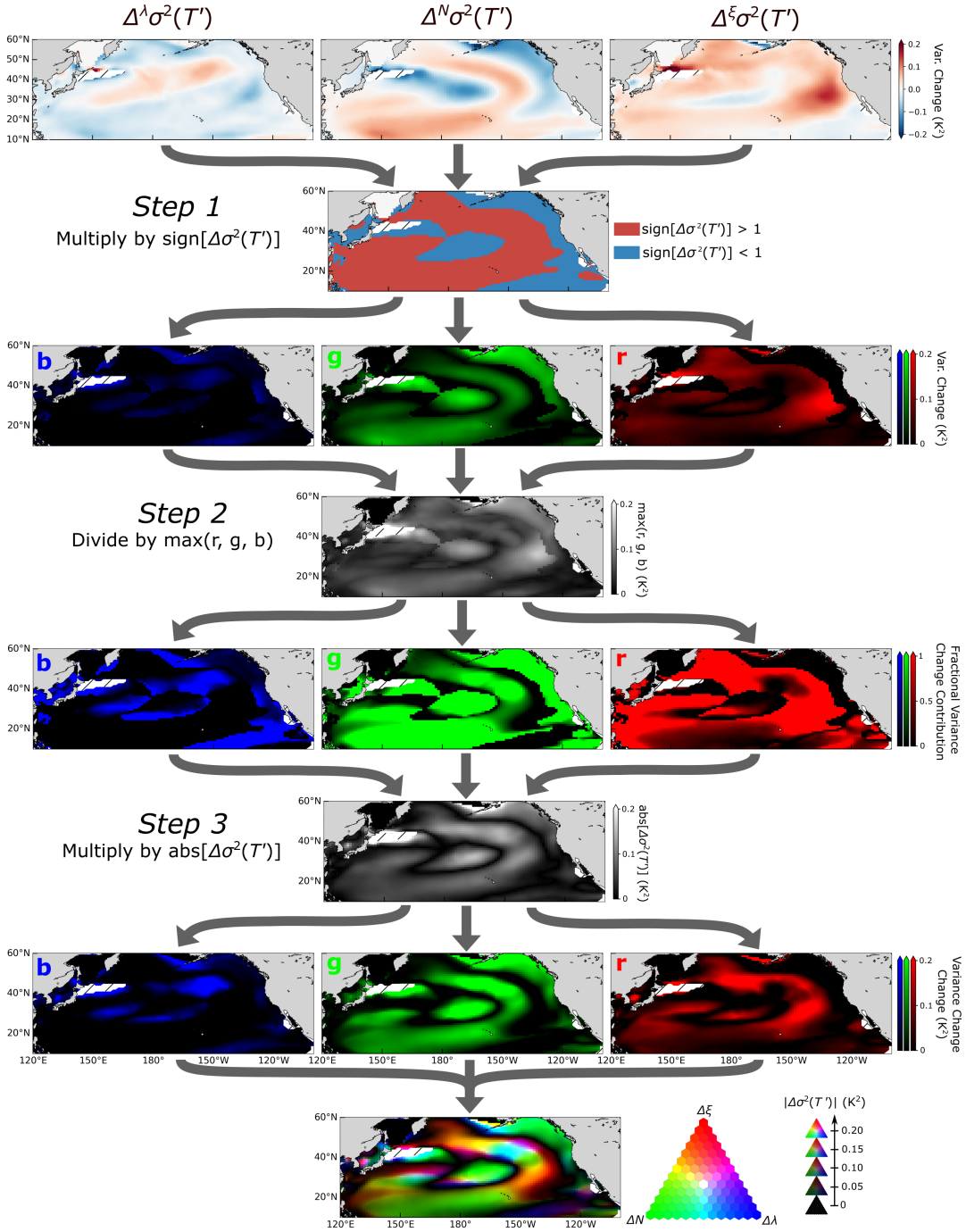

Supplementary Figure S7: Construction of Figure 4h. *Step 1*: The variance changes due to each driver $\Delta^x\sigma^2(T')$ are first multiplied by the sign of the total variance change $\Delta\sigma^2(T') = \Delta^{\lambda}\sigma^2(T') + \Delta^{N}\sigma^2(T') + \Delta^{\xi}\sigma^2(T')$. That isolates where each driver is most "contributing" to the overall variance change (i.e., a driver is not considered to contribute to the variance change if they are of opposite signs at a given grid point). Each driver is assigned a color channel: blue for $\Delta^{\lambda}\sigma^2(T')$, green for $\Delta^{N}\sigma^2(T')$, and red for $\Delta^{\xi}\sigma^2(T')$. *Step 2*: Each channel is divided by the maximum value among the red, green, and blue channels at each grid point to normalize the variance change contributions. *Step 3*: Each channel is multiplied by the absolute value of $\Delta\sigma^2(T')$ so that when combined the "brightness" of the combined RGB image corresponds to the magnitude of $\Delta\sigma^2(T')$.